Journal of Science and Technology – Engineering and Technology for Sustainable Development
Volume 36, Issue 1, March 2026, 009-016

Synthesis of ZnO/Al_2O_3 from Bohemite via the Impregnation Method and Its Potential as an Activator in Rubber Vulcanization

Nghiem Thi Thuong, Nguyen Minh Tien, Nguyen Hoang Trung, Nguyen Han Long*
Hanoi University of Science and Technology, Ha Noi, Vietnam
** Corresponding author email: long.nguyenhan@hust.edu.vn*

Abstract

The study synthesized and investigated ZnO/Al_2O_3 composites as potential activators for rubber vulcanization. Al_2O_3 was initially prepared from boehmite, followed by ZnO deposition via wet impregnation with varying $Zn(NO_3)_2$ solution concentrations. This approach yielded a series of composite 10%, 15%, 20%, 25%, 30%, 35%, and 40% ZnO. Comprehensive characterization was conducted using X-ray diffraction (XRD), Brunauer-Emmett-Teller (BET) surface area analysis, particle size distribution, and scanning electron miscroscopy (SEM). XRD analysis confirmed the formation of γ-Al_2O_3 and the deposition of nano-sized ZnO onto the Al_2O_3 surface. SEM examination demonstrated that the porous structure of Al_2O_3 was preserved, particularly in the in 20% ZnO/Al_2O_3 sample, which was therefore was selected for the natural rubber (NR) vulcanization study. The NR compound containing 10 phr of 20% ZnO/Al_2O_3 exhibited a steady torque increase over time, with an extended optimal cure time compared to compounds containing conventional ZnO (2 phr) and Al_2O_3 (8 phr) individually and their physical mixture. Despite the longer cure time, this formulation achieved superior tensile strength and elongation at break. These improvements are attributed to the synergistic effects between ZnO and Al_2O_3, where ZnO promotes crosslink formation while Al_2O_3 helps suppress the overcuring typically caused by ZnO.

Keywords: Activator, impregnation method, natural rubber, rubber vulcanization, ZnO/Al_2O_3.

1. Introduction

Zinc oxide (ZnO) is widely used in the rubber industry as an activator in the vulcanization process. Its presence significantly enhances the vulcanization rate and promotes the formation of cross-linked networks within the rubber matrix. The benefits of using ZnO extend beyond reducing curing time; it also enables vulcanization at lower temperatures and allows for a reduced sulfur content compared to traditional formulations. Additionally, ZnO improves the mechanical properties of vulcanized rubber, particularly its tensile strength.

Despite its beneficial effects on rubber properties, ZnO poses significant environmental concerns. It is recognized as a pollutant with high carcinogenic potential for aquatic organisms. At the end of a rubber product's service life, ZnO may be released into the environment through degradation or leaching from landfills. Elevated concentrations of ZnO have been detected in wastewater treatment plants, posing toxicity risks to aquatic life. Another major source of environmental ZnO is tire wear during regular use.

Given the growing global emphasis on environmental protection and green chemistry, reducing ZnO emissions has become a critical concern. Consequently, researchers worldwide have been exploring alternative approaches to replace conventional ZnO in the rubber industry. Recent studies have focused on ZnO nanoparticles and modified ZnO as activators in the vulcanization of natural rubber (NR). For instance, the research group led by Suchismita Sahoo [1–3] reported that replacing conventional ZnO with ZnO nanoparticles (30–50 nm) in formulations for NR, polychloroprene rubber, and nitrile rubber enhanced thermal resistance and improved mechanical properties. In another study, Panampilly and colleagues [4] synthesized ZnO nanoparticles ranging from 20–90 nm in size, with a specific surface area of 9.56 m^2/g. When incorporated at 0.5 parts by weight into vulcanization formulations, these nanoparticles achieved curing performance and efficiency comparable to 5 parts by weight of conventional micro-sized ZnO. Qin and co-researchers [5] used 5 nm ZnO nanoparticles modified with octyl amide to replace micro-sized ZnO, demonstrating faster vulcanization rates and enhanced rubber properties.

Roy and colleagues [6] further improved the efficiency of ZnO by modifying its surface with stearic acid and bis[3-(triethoxysilyl)propyl] tetrasulfide (Si-69), resulting in increased tensile strength, crosslink density, and storage modulus. Alam *et al.* [7] investigated a dual-activator system combining ZnO and MgO, demonstrating that substituting 60% of ZnO with MgO improved both vulcanization efficiency and the final material properties.

Further research [8] has explored the synergistic effects of $Ca(OH)_2$, MgO, and ZnO in various rubber

p-ISSN 3093-3242
e-ISSN 3093-3579
https://doi.org/10.51316/jst.188.etsd.2026.36.1.2
Received: Apr 25, 2025; Revised: Aug 20, 2025;
Accepted: Aug 26, 2025; Online: Feb 5, 2026.

systems. The results indicated that $Ca(OH)_2$ is particularly suitable for styrene-butadiene rubber, while MgO proved effective in both styrene-butadiene and sodium styrene-butadiene systems. These studies highlight the growing interest in alternative activator systems that minimize environmental impact without compromising performance.

ZnO-based composites dispersed on other metal oxides such as TiO_2 [9], CuO [10], zeolites [11], and Al_2O_3 [12] have found applications in fields such as photocatalysis, solar cells, gas sensors, and supercapacitors. However, their use as vulcanization activators in rubber processing remains largely unexplored. For example, Ji-Fang Fu [13], evaluated activated Al_2O_3 as a promising reinforcing agent for rubber materials due to its high surface area, thermal stability, and low cost.

Based on published studies, ZnO nanoparticles dispersed on Al_2O_3 show significant potential to enhance mechanical properties, improve production efficiency, and reduce environmental impact. This research is divided into two parts: the first focuses on the synthesis of ZnO nanoparticles on γ-Al_2O_3, and the second investigates the effectiveness of the resulting ZnO/γ-Al_2O_3 composite as a potential activator for rubber vulcanization.

2. Experiments

2.1. Materials

The materials used in this study included natural rubber of grade SVR3L. The chemical reagents employed were zinc nitrate hexahydrate ($Zn(NO_3)_2.6H_2O$), boehmite (AlOOH), stearic acid ($CH_3(CH_2)_{16}COOH$), N-tert-butyl-2-benzothiazolesulfenamide (TBBS, $C_{11}H_{14}N_2S_2$), sulfur (S), 90% ethanol, and deionized water.

2.2. Synthesis of γ-Al_2O_3

γ-Al_2O_3 was synthesized from boehmite. First, the boehmite was washed three times with hot deionized water (95 °C), followed by vacuum filtration to remove impurities. The filtered sample was then dried at 120 °C for 3 hours. After drying, the material was ground and calcined at 300 °C for 5 hours, followed by a second calcination at 600 °C for an additional 5 hours.

2.3. Synthesis of ZnO/γ-Al_2O_3

ZnO/γ-Al_2O_3 was synthesized via the impregnation method using a $Zn(NO_3)_2$ solution and the previously prepared γ-Al_2O_3. Initially, γ-Al_2O_3 was mixed with $Zn(NO_3)_2$ solution, and the mixture was placed in trays and dried in an oven at 120 °C for 3 hours to remove physically adsorbed water and stabilize the structure. After drying, the mixture was impregnated a second time with the remaining $Zn(NO_3)_2$ solution until no liquid remained. The resulting material was then dried again at 120 °C for 3 hours, followed by calcination at 600 °C for 3 hours to obtain the final ZnO/γ-Al_2O_3 composite.

2.4. Rubber Vulcanization

Prior to vulcanization, the ZnO/γ-Al_2O_3 composite synthesized under optimal conditions was further processed by adding a dispersing additive (stearic acid), ethanol, and distilled water. The mixture was then dried at approximately 100 °C until a constant weight was achieved. The vulcanization formulation consisted of NR(100 phr), sulfur (3 phr), TBBS (0.7 phr), stearic acid (1 phr), and ZnO/γ-Al_2O_3. Rubber compounds were prepared using the melt blending method in a Labo Plastomil 4M150 internal mixer, followed by a curing in a hot press at 150 °C for the optimal cure time.

2.5. Characterizations

The nanomaterial structure was characterized and evaluated using several techniques, including X-ray diffraction (XRD), scanning electron microscopy (SEM), energy-dispersive X-ray spectroscopy (EDX), laser scattering, and Brunauer-Emmett-Teller (BET) nitrogen adsorption-desorption analysis. XRD patterns of the synthesized samples were recorded using a Bruker D8 Advance diffractometer with CuKα radiation (λ = 1.5418 Å), operating at 40 kV and 40 mA. The scan range was 10°–70° (2θ) with a step size of 0.02°. Surface morphology and elemental composition were analyzed using a Hitachi S-4800 SEM equipped with an EDX system. SEM images were captured at magnifications ranging from 100× to 10,000×, with an accelerating voltage of 5 kV. Particle size distribution was determined using a HORIBA LA-950 laser scattering particle size analyzer. Nitrogen adsorption-desorption isotherms were measured using a Micromeritics ASAP 2060 instrument to analyze the material's specific surface area and pore size distribution.

The curing behavior of the rubber vulcanizates was characterized using a rheometer in accordance with ASTM D5289. Measurement was performed at 150 °C for 60 min. The tensile strength of the rubber was determined by stretching the sample at a constant crosshead speed of 200 mm/min at room temperature. Test specimens, approximately 1 mm thick, were cut using a dumbbell-shaped No.7 cutter in accordance with the JIS K6251 standard.

3. Result and Discussion

3.1. Characterization of Synthesized γ-Al_2O_3

Fig. 1 shows the XRD patterns of boehmite before and after calcination. The XRD analysis of the raw boehmite sample revealed characteristic diffraction peaks at 2θ equal 14.4° and 2θ equal 28.2°, corresponding to the crystalline structure of boehmite. When compared with the nano-boehmite sample reported by Jing Yang [14], the synthesized boehmite in this study exhibits similar peak positions, confirming that the crystalline phase remains unchanged.

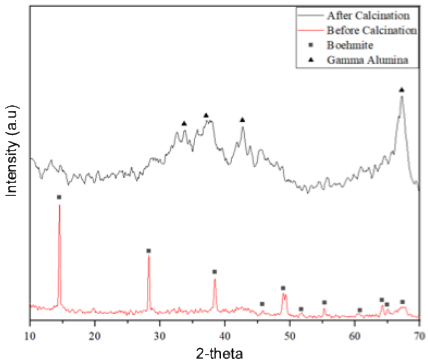

Fig. 1. XRD of boehmite before and after calcination

However, significant differences are evident in crystallinity and purity. The synthesized nano-boehmite exhibits sharp, well-defined diffraction peaks with high intensity, indicating excellent crystallinity. Additionally, no extra peaks corresponding to gibbsite or other aluminum oxide phases were detected, suggesting a high level of purity. These observations are consistent with the findings of Jing Yang [14], who also reported a high-purity nano-boehmite phase with excellent crystallinity.

When the boehmite sample was calcined at 600 °C for 5 hours, XRD analysis confirmed the transformation into γ-Al_2O_3. This was evidenced by the disappearance of the boehmite peaks and the emergence of broad, low-intensity peaks characteristic of γ-Al_2O_3 at 2θ equal 31.9° and 2θ equal 67.0°. The XRD pattern of γ-Al_2O_3 is characterized by broad, low-intensity, and less well-defined peaks, indicating an incomplete crystalline structure.

The structural characterization of γ-Al_2O_3 was further evaluated through BET isotherm analysis. The BET surface area of the γ-Al_2O_3 sample was 208.77 m^2/g. Based on the nitrogen adsorption isotherm (Fig. 2), at p/p_0 equal 0.01, the nitrogen adsorption capacity reached approximately 38.89 cm^3/g, increasing to 328.53 cm^3/g at p/p_0 equal 0.99. The pore size distribution ranged from 7 to 400 Å, with a concentration in the 20–40 Å range. These superior characteristics explain why γ-Al_2O_3 is widely utilized in adsorption and catalysis applications and suggest that it may also be suitable for dispersion with other compounds, such as ZnO.

3.2. Characterization of ZnO/γ-Al_2O_3

Fig. 3 shows the XRD patterns of the synthesized ZnO/γ-Al_2O_3 composites. Characteristic diffraction peaks are observed at 2θ equal 32.14°, 36.67°, and 68.38°, corresponding to the ZnO crystalline phase. As the amount of impregnated $Zn(NO_3)_2$ solution increased, the intensity of the ZnO diffraction peaks also increased, indicating greater ZnO loading onto γ-Al_2O_3 ranging from 10% ZnO/γ-Al_2O_3 to 40% ZnO/γ-Al_2O_3.

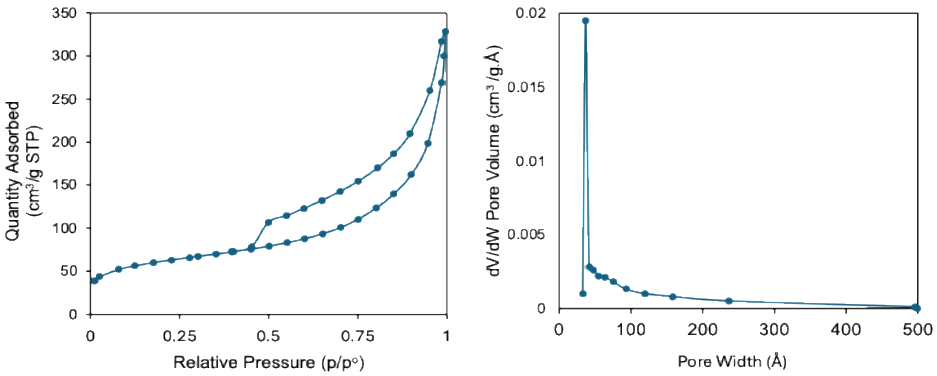

Fig. 2. Nitrogen adsorption-desorption isotherm and pore size distribution curve of the γ-Al_2O_3 sample

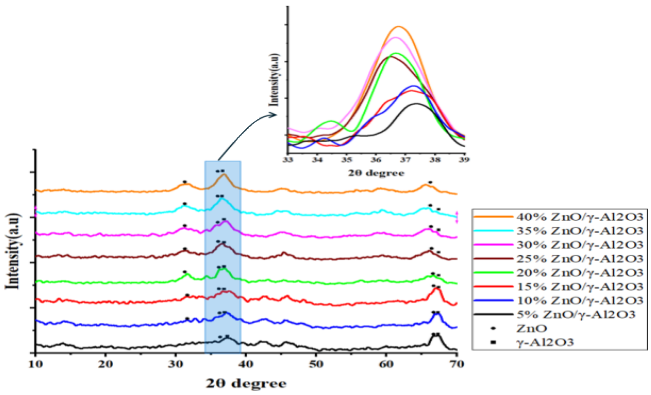

Fig. 3. XRD patterns of ZnO/γ-Al_2O_3 composites with different ZnO contents

The diffraction peaks in the 10% and 15% ZnO/γ-Al_2O_3 samples exhibit broad bases and low sharpness, suggesting that ZnO crystals are poorly developed and that a significant portion remains in the amorphous state. This indicates that at low $Zn(NO_3)_2$ concentrations, the formation of nano-ZnO crystals on the γ-Al_2O_3 surface is incomplete.

For the ZnO/γ-Al_2O_3 samples with increasing ZnO content (20%, 25%, 30%, 35%, and 40%), the diffraction peaks become sharper and more intense compared to the 10% and 15% ZnO/γ- Al_2O_3 samples. This change indicates an improvement in ZnO crystallization. Notably, the 40% ZnO/γ-Al_2O_3 sample exhibits the sharpest and most well-defined peaks, signifying the highest degree of crystallinity among the studied samples.

The crystallite size of ZnO was determined using Scherrer's equation from XRD data, as shown in Table 1. The results indicate that the crystallite size of ZnO is small (below 4 nm) but increases as ZnO content increases. Based on BET and pore size analyses, the pore size of γ-Al_2O_3 predominantly ranges from 20 to 40 Å (2–4 nm). Therefore, nano-ZnO crystals are likely confined within the nanopores of the γ-Al_2O_3 structure. This suggests that a significant portion of ZnO nanoparticles may be embedded within the porous network of γ-Al_2O_3.

Table 1. Crystalline size of synthesized ZnO/γ-Al_2O_3

Sample	Particle size (nm)
5% ZnO/γ-Al_2O_3	0.76
10% ZnO/γ-Al_2O_3	1.57
15% ZnO/γ-Al_2O_3	1.64
20% ZnO/γ-Al_2O_3	1.98
25% ZnO/γ-Al_2O_3	2.26
30% ZnO/γ-Al_2O_3	2.67
35% ZnO/γ-Al_2O_3	3.01
40% ZnO/γ-Al_2O_3	3.42

To evaluate the size of ZnO/γ-Al_2O_3 composites, particle size distribution analysis was performed using laser scattering methodology. Fig. 4 presents the particle size distributions of pure γ-Al_2O_3 and ZnO/γ-Al_2O_3 composites containing 10%, 20%, and 40% ZnO loadings. Purely γ-Al_2O_3 exhibited an average particle size of 40.8 μm, with a broad distribution ranging from 1 to 100 μm, indicating a heterogeneous particle morphology comprising both fine and coarse fractions.

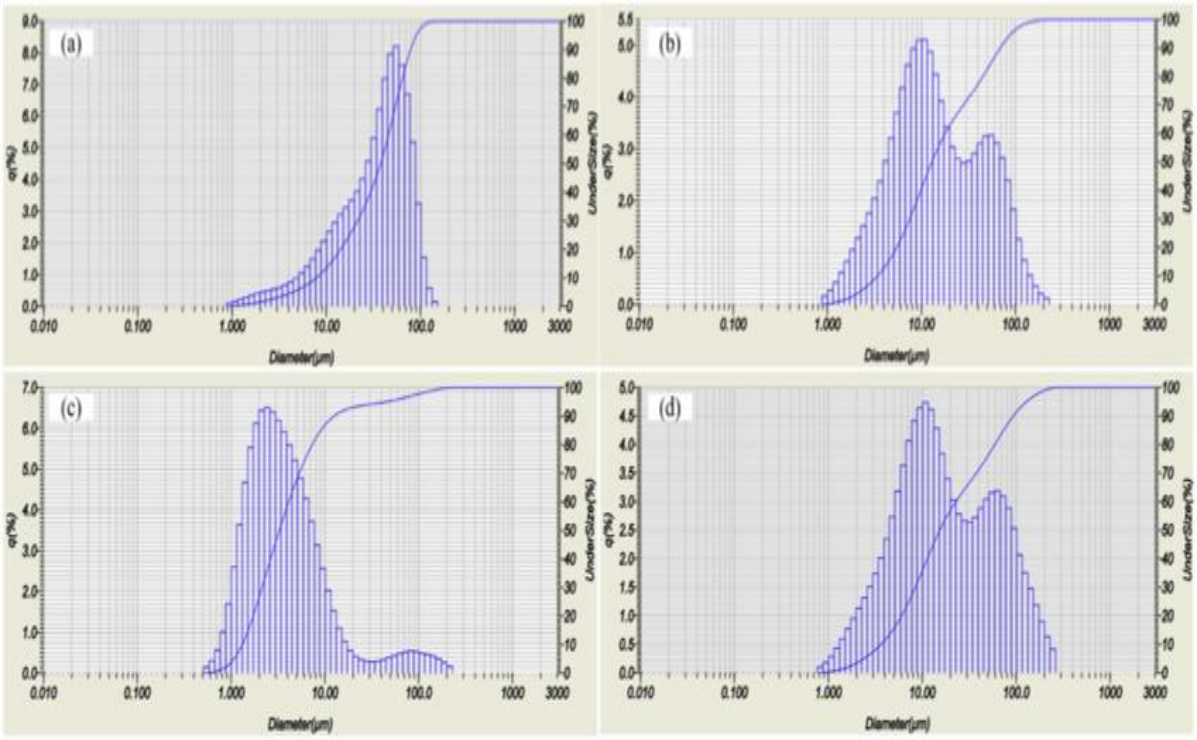

Fig. 4. Particle size distribution of ZnO/γ-Al_2O_3
(a) γ-Al_2O_3; (b) 10% ZnO/γ-Al_2O_3; (c) 20% ZnO/γ-Al_2O_3; (d) 40% ZnO/γ-Al_2O_3

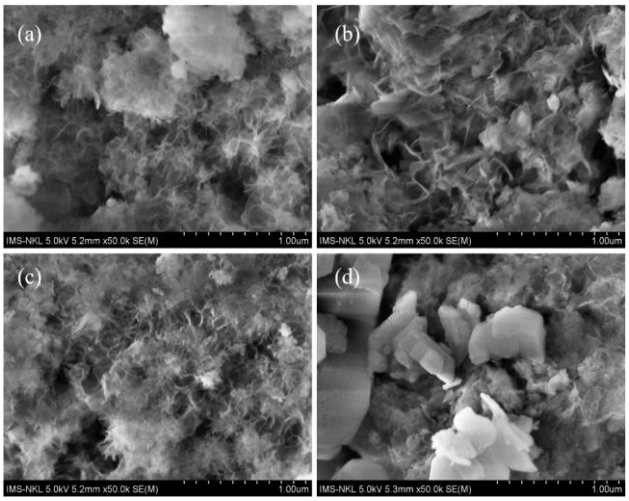

Fig 5. SEM images of (a) γ-Al_2O_3, (b) 10% ZnO/γ-Al_2O_3, (c) 20% ZnO/γ-Al_2O_3, (d) 40% ZnO/γ-Al_2O_3

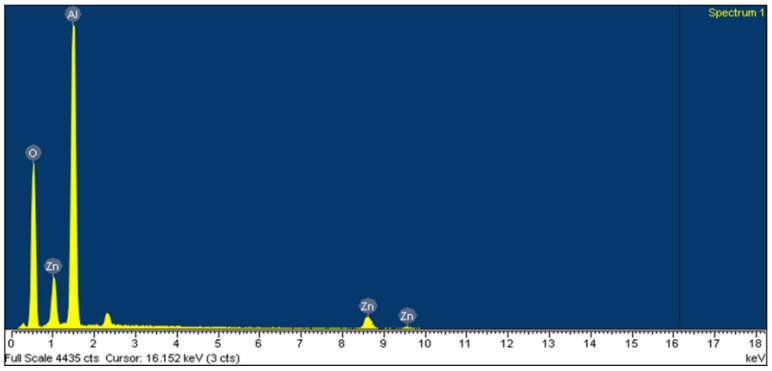

Fig. 6. EDX analysis result of the 20% ZnO/γ-Al_2O_3 sample

The 10% ZnO/γ-Al_2O_3 composite showed a substantial shift in particle size distribution, exhibiting bimodal characteristics with distinct peaks at approximately 10 µm and 50 µm. This bimodal pattern suggests that ZnO incorporation onto the γ-Al_2O_3 surface promotes particle agglomeration or induces structural modifications at the interface.

At 20% ZnO loading, the average particle size decreased markedly to 9.6 µm, representing a significant reduction compared to pure γ-Al_2O_3. Additionally, the size distribution narrowed considerably, with particles predominantly concentrated in the smaller size range. These findings suggest that increased ZnO content promotes enhanced particle size uniformity within the ZnO/γ-Al_2O_3 composite.

The 40% ZnO loading, the composite exhibited a further reduction particle size, confirming that high ZnO loading substantially influences particle size distribution, leading to decreased average particle size and improved size uniformity.

SEM was employed to investigate the morphological characteristics of ZnO/γ-Al_2O_3 composite. Fig. 5 displays SEM images of pure γ-Al_2O_3 and ZnO/γ-Al_2O_3 composites with varying ZnO loadings. Progressive increases in ZnO content resulted in significantly alternations to surface morphology and ZnO distribution. Pure γ-Al_2O_3 exhibited disordered crystalline structure characterized by a dense, complex porous network, which contributes to its high specific surface area. However, this structural disorder may hinder the uniform dispersion of secondary phases, such as ZnO. In the 10% ZnO/γ-Al_2O_3 sample, ZnO particles were observed on the surface with a heterogeneous distribution, while the majority of the original porous framework remaining intact. At 20% ZnO loading, the γ-Al_2O_3 pores demonstrated sufficient capacity to accommodate ZnO particles, although incomplete pore filling indicated a non-uniform distribution. Despite this heterogeneity, ZnO particle size maintained relatively small, and the overall porous network was preserved - achieving an optimal balance between porosity and active phase dispersion.

The 40% ZnO/γ-Al_2O_3 composite revealed the formation of larger ZnO crystallites with localized, uneven distribution, leading to a reduction in porous network efficiency and surface area. These observations confirm that increasing ZnO content significantly

influences the material's structure. Comparative analysis identified the 20% ZnO/γ-Al_2O_3 sample as the most optimal, effectively preserving the porous structure while achieving balanced and efficient ZnO dispersion.

To confirm the actual ZnO loading in the 20% ZnO/γ-Al_2O_3 sample, EDX analysis was performed. Fig. 6 presents the elemental composition profile of the 20% ZnO/γ-Al_2O_3 sample. The EDX results revealed the presence of oxygen (O) at 52.41 wt%, aluminum (Al) at 36.17 wt%, and zinc (Zn) at 11.42 wt%. Based on this data, the ZnO content was calculated to be 17.72 wt%, with γ-Al_2O_3 accounting for 82.28 wt%. This experimental result shows excellent agreement with the theoretical ZnO loading of 20%, thereby validating the accuracy and reproducibility of the synthesis method employed.

Table 2. EDX result of 20% ZnO/γ-Al_2O_3 sample

Element	Mass (%)	Particle (%)
Zn	11.42	3.65
Al	36.17	27.98
O	52.41	68.37

To investigate the adsorption properties of the synthesized ZnO/γ-Al_2O_3, BET surface area analysis was conducted. Fig. 7 presents the nitrogen adsorption-desorption isotherms and pore size distributions for pure γ-Al_2O_3, and ZnO/γ-Al_2O_3 composites containing 10%, 15%, and 20% ZnO loadings.

BET analysis revealed that all ZnO/γ-Al_2O_3 samples exhibited Type IV adsorption-desorption isotherms, characteristic of mesoporous materials according to IUPAC classification. Additionally, the presence of H3-type hysteresis loops indicates non-uniform pore geometry, typically associated with plate-like or slit-shaped pore structures.

The specific surface areas were determined as follows: pure γ-Al_2O_3 (208.77 m^2/g), 10% ZnO/γ-Al_2O_3 (204.64 m^2/g), 15% ZnO/γ-Al_2O_3 (198.91 m^2/g), 20% ZnO/γ-Al_2O_3 (200.07 m^2/g). The pore size distribution for all samples ranged from 20 to 500 Å, confirming the preservation of the mesoporous framework upon ZnO incorporation.

Despite the progressive increases in ZnO loading, the specific surface area and pore size distribution remained relatively stable, indicating successful application of the impregnation method. This approach effectively prevented pore blockage by ZnO particles, thereby maintaining the textural properties of γ-Al_2O_3. These findings demonstrate that the wet impregnation technique is an effective strategy for ZnO deposition while preserving the mesoporous chacteristics essential for catalytic applications.

3.3. Curing Characteristic

To assess the effectiveness of ZnO/γ-Al_2O_3 as a vulcanization activator for NR, the 20% ZnO/γ-Al_2O_3 sample was selected based on its superior homogenous ZnO distribution on the Al_2O_3 support. This sample was incorporated at a loading of 10 phr, corresponding to approximately 2 phr of ZnO and 8 phr of Al_2O_3. For comparison, three additional formulations were prepared, in which ZnO/γ-Al_2O_3 was replaced with (i) conventional micro-ZnO (2 phr); (ii) γ-Al_2O_3 (8 phr), and (iii) a physical mixture of ZnO (2 phr) and γ-Al_2O_3 (8 phr).

Fig. 8 presents the curing curves of the vulcanized NR samples. The NR compounds containing conventional ZnO and the ZnO/γ-Al_2O_3 mixture exhibited increasing torque values during the first 14 and 16 min of curing, respectively, followed by a progressive decline. This torque reversion is indicative of overcuring behavior, which is typically attributed to thermal degradation of the crosslinked network under prolonged exposure to elevated temperature and pressure. Such degradation often leads to a deterioration in mechanical properties. The optimal cure time (t_{90}) for NR formulations using ZnO and the ZnO/γ-Al_2O_3 mixture were determined to be 10 and 16 min, respectively.

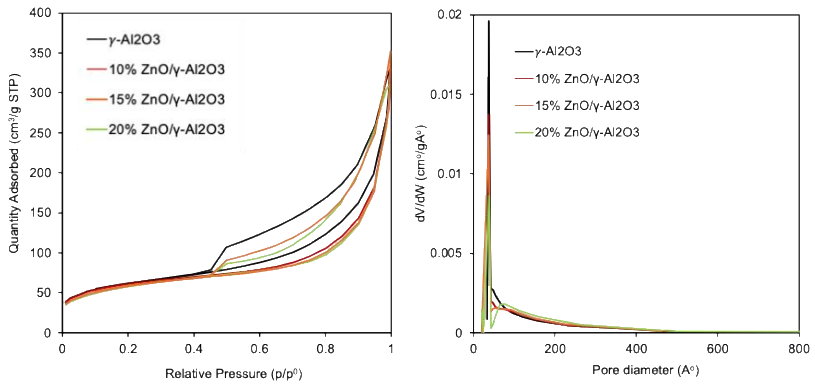

Fig. 7. Nitrogen adsorption-desorption isotherms and pore size distribution of γ-Al_2O_3, 10% ZnO/γ-Al_2O_3, 15% ZnO/γ-Al_2O_3, and 20% ZnO/γ-Al_2O_3 samples

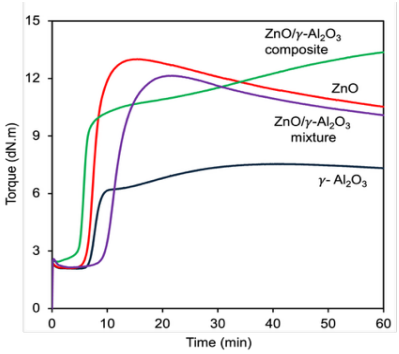

Fig. 8. Curing curves of NR vulcanized with ZnO γ-Al_2O_3, 20% ZnO/γ-Al_2O_3 composite and ZnO/γ-Al_2O_3 mixture

In contrast, NR samples vulcanized with 10 phr of 20% ZnO/γ-Al_2O_3 and with 8 phr of γ-Al_2O_3 exhibited a continuous increase in torque that extended beyond the optimal vulcanization stage. This behavior indicates sustained crosslink formation throughout the vulcanization process. However, this enhanced crosslinking performance was accompanied by a significant extension in t_{90}. Specifically, t_{90} increased from approximately 22 min for the sample containing only Al_2O_3 to 44 min for the sample incorporating 10 phr of 20% ZnO/γ-Al_2O_3. This prolonged cure time can be attributed to the microporous structure of γ-Al_2O_3, which absorbs curing accelerator during initial mixing and gradually releases them at elevated temperatures. Notably, the ZnO/γ-Al_2O_3 composite formulations exhibited a slightly reduced scorch time compared to the conventional ZnO-only system. This acceleration in the early-stage stages of vulcanization is likely due to localized thermal effects resulting from the enhanced thermal conductivity of γ-Al_2O_3, which facilitates more rapid initiation of the crosslinking reaction at the rubber-filler interface.

3.4. Tensile Strength and Hardness

Fig. 9 presents the stress-strain curves for the vulcanized NR samples. The NR vulcanized with ZnO and the ZnO/γ-Al_2O_3 mixture achieved stresses at break of 14.9 and 12 MPa, respectively, both exhibiting pronounced strain-induced crystallization during deformation. In contrast, the NR sample vulcanized with 8 phr Al_2O_3 alone showed significantly inferior mechanical performance, reaching only 4 MPa stress at break with minimal evidence of strain-induced crystallization. This reduced mechanical performance is likely due to insufficient crosslink formation in the vulcanized NR network. These findings are further supported by the lowest values of M_{100}, M_{300} and shore *A* hardness recorded for the NR sample vulcanized with Al_2O_3, as shown in Table 3.

Remarkably, the NR sample vulcanized with the 20% ZnO/Al_2O_3 composite achieved superior mechanical properties, exhibiting a stress at break of 16.1 MPa and a strain at break of 1000%, while maintaining relatively low values for M_{100}, M_{300}, and shore *A* hardness. These results represent a significant improvement over formulations conventional ZnO, γ-Al_2O_3, and their physical mixture formulations. The enhanced performance can be attributed to the synergistic interaction between ZnO and γ-Al_2O_3, where the γ-Al_2O_3 component likely contributes to improved flexibility of the rubber matrix while preserving effective vulcanization activation. These findings demonstrate that the ZnO/γ-Al_2O_3 composite represents a promising alternative activator for NR vulcanization.

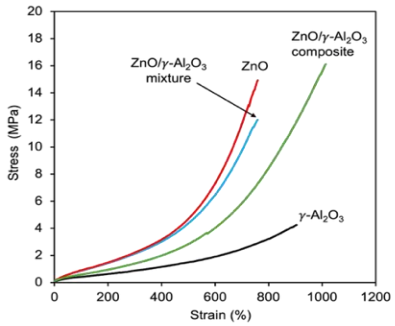

Fig. 9. Stress-strain curves of vulcanized NR samples vulcanized with ZnO γ-Al_2O_3, 20% ZnO/γ-Al_2O_3 composite, and ZnO/γ-Al_2O_3 mixture

Table 3. M_{100}, M_{300}, and shore *A* hardness

Sample	M_{100} (MPa)	M_{300} (MPa)	Hardness (shore *A*)
ZnO	0.89	2.21	41
Al_2O_3	0.42	0.88	22
ZnO/γ-Al_2O_3 mixture	0.58	1.39	39
ZnO/γ-Al_2O_3 composite	0.87	2.12	34

4. Conclusion

In this study, ZnO/γ-Al_2O_3 composite was successfully synthesized via a wet impregnation method, with systematic variation in ZnO loading on the Al_2O_3 support. The formation of nano-sized ZnO was confirmed, and the 20% ZnO/γ-Al_2O_3 sample demonstrated an optimal, homogeneous distribution of ZnO across the Al_2O_3 surface. BET surface area analysis indicated that ZnO was primarily deposited on the external surface rather than within the mesopores of Al_2O_3. The 20% ZnO/γ-Al_2O_3 composite was subsequently evaluated as a vulcanization activator for NR. It not only accelerated the vulcanization process but also significantly enhanced the mechanical properties of NR compared to formulations using micro-ZnO or γ-Al_2O_3 alone or their physical mixture. These findings

highlight the potential of ZnO/γ-Al_2O_3 as a novel and effective activator for NR vulcanization.

Acknowledgements.

This research is funded by Vietnam Ministry of Education and Traning (MOET) under grant number B2024-BKA-06.

References

[1] S. Sahoo, S. Kar, A. Ganguly, M. Maiti, A. K. Bhowmick, Synthetic zinc oxide nanoparticles as curing agent for polychloroprene, Polymers and Polymer Composites, vol. 16, iss. 3, pp. 193–198, 2008. https://doi.org/10.1177/096739110801600304

[2] S. Sahoo, M. Maiti, A. Ganguly, J.J.George, A. K. Bhowmick, Effect of zinc oxide nanoparticles as cure activator on the properties of natural rubber and nitrile rubber, Journal of Applied Polymer Science, vol. 105, iss. 4, pp. 2407–2415, May 2007. https://doi.org/10.1002/app.26296

[3] S. Sahoo, A. K. Bhowmick, Influence of ZnO nanoparticles on the cure characteristics and mechanical properties of carboxylated nitrile rubber, Journal of Applied Polymer Science, vol. 106, iss. 5, pp. 3077–3083, Aug. 2007. https://doi.org/10.1002/app.24832

[4] B. Panampilly and S. Thomas, Nano ZnO as cure activator and reinforcing filler in natural rubber, Polymer Engineering and Science, vol. 53, iss. 6, pp. 1337–1346, Jun. 2013. https://doi.org/10.1002/pen.23383

[5] X. Qin, H. Xu, G. Zhang, J. Wang, Z. Wang, Y. Zhao, Z. Wang, T. Tan, M. R. Bockstaller, L. Zhang, and K. Matyjaszewski, Enhancing the performance of rubber with nano ZnO as activators, ACS Applied Materials and Interfaces, vol. 12, iss. 42, pp. 48007–48015, Oct. 2020. https://doi.org/10.1021/acsami.0c15114

[6] K. Roy, M. N. Alam, S. K. Mandal, and S. C. Debnath, Surface modification of sol–gel derived nano zinc oxide (ZnO) and the study of its effect on the properties of styrene–butadiene rubber (SBR) nanocomposites, Journal of Nanostructure Chemistry, vol. 4, Sep. 2014, Art. no. 133. https://doi.org/10.1007/s40097-014-0127-9

[7] M. N. Alam, V. Kumar, and S. S. Park, Advances in rubber compounds using ZnO and MgO as co-cure activators, Polymers, vol. 14, Dec. 2022, Art. no. 5289. https://doi.org/10.3390/polym14235289

[8] M. Feldstein, P. Orlovsky, and B. Dogadkin, The role of metal oxides as activators of vulcanization, Rubber Chemistry and Technology, vol. 31, iss. 3, pp. 526–538, Jul. 1958. https://doi.org/10.5254/1.3542304

[9] W. Ahmad, U. Mehmood, A. Al-Ahmed, F. A. Al-Sulaiman, M. Z. Aslam, M. S. Kamal, and R. A. Shawabkeh, Synthesis of zinc oxide/titanium dioxide (ZnO/TiO_2) nanocomposites by wet incipient wetness impregnation method and preparation of ZnO/TiO_2 paste using poly(vinylpyrrolidone) for efficient dye-sensitized solar cells, Electrochimica Acta, vol. 222, pp. 473–480, Dec. 2016. https://doi.org/10.1016/j.electacta.2016.10.200

[10] S. Das and C. Vimal, An overview of the synthesis of CuO-ZnO nanocomposite for environmental and other applications, Nanotechnology Reviews, vol. 7, iss. 3, pp. 267–282, Apr. 2018. https://doi.org/10.1515/ntrev-2017-0144

[11] H. Tehubijuluw, R. Subagyo, Y. Kusumawati, and D. Prasetyoko, The impregnation of ZnO onto ZSM-5 derived from red mud for photocatalytic degradation of methylene blue, Sustainable Environment Research, vol. 32, Jan. 2022, Art. no. 4. https://doi.org/10.1186/s42834-021-00113-8

[12] N. Hidayah, M. Mustapha, H. Ismail, and M. Kamarol, Linear low-density polyethylene/silicone rubber nanocomposites: optimization of parameters and effect on electrical properties, Journal of Elastomers and Plastics, vol. 50, iss. 1, pp. 36–57, Apr. 2017. https://doi.org/10.1177/0095244317704983

[13] J. F. Fu, L. Y. Chen, H. Yang, Q. D. Zhong, L. Y. Shi, W. Deng, X. Dong, Y. Chen, and G. Z. Zhao, Mechanical properties, chemical and aging resistance of natural rubber filled with nano Al_2O_3, Polymer Composites, vol. 33, no. 3, pp. 404–411, Feb. 2012. https://doi.org/10.1002/pc.22162

[14] Yang, Jing, Frost, L. Ray, Synthesis and Characterization of Boehmite Nanofibers, Research Letters in Inorganic Chemistry, vol. 2008, iss. 1, Oct. 2008, Art. no. 602198. https://doi.org/10.1155/2008/602198